Available online at www.sciencedirect.com
ScienceDirect
Journal of Magnesium and Alloys xxx (xxxx) xxx
www.elsevier.com/locate/jma

Full Length Article

Bioinspired fish-scale-like magnesium composites strengthened by contextures of continuous titanium fibers: Lessons from nature

Yanyan Liu[a,b], Qin Yu[c], Guoqi Tan[a,b], Mingyang Zhang[a,b], Enling Tang[d], Shaogang Wang[a], Zengqian Liu[a,b,*], Qiang Wang[e,**], Zhefeng Zhang[a,b], Robert O. Ritchie[c]

[a] *Institute of Metal Research, Chinese Academy of Sciences, Shenyang 110016, China*
[b] *School of Materials Science and Engineering, University of Science and Technology of China, Hefei 230026, China*
[c] *Department of Materials Science and Engineering, University of California Berkeley, Berkeley, CA 94720, USA*
[d] *Key Laboratory of Transient Physical Mechanics and Energy Conversion Materials of Liaoning Province, Shenyang Ligong University, Shenyang 110159, China*
[e] *Liaoning Provincial Key Laboratory of Oral Diseases, School and Hospital of Stomatology, China Medical University, Shenyang 110001, China*

Received 19 January 2021; received in revised form 27 May 2021; accepted 19 June 2021
Available online xxx

Abstract

Natural fish scales demonstrate outstanding mechanical efficiency owing to their elaborate architectures and thereby may serve as ideal prototypes for the architectural design of man-made materials. Here bioinspired magnesium composites with fish-scale-like orthogonal plywood and double-Bouligand architectures were developed by pressureless infiltration of a magnesium melt into the woven contextures of continuous titanium fibers. The composites exhibit enhanced strength and work-hardening ability compared to those estimated from a simple mixture of their constituents at ambient to elevated temperatures. In particular, the double-Bouligand architecture can effectively deflect cracking paths, alleviate strain localization, and adaptively reorient titanium fibers within the magnesium matrix during the deformation of the composite, representing a successful implementation of the property-optimizing mechanisms in fish scales. The strength of the composites, specifically the effect of their bioinspired architectures, was interpreted based on the adaptation of classical laminate theory. This study may offer a feasible approach for developing new bioinspired metal-matrix composites with improved performance and provide theoretical guidance for their architectural designs.

Keywords: Magnesium composites; Bioinspired materials; Fish scales; Bouligand-type architecture; Structural reorientation.

1. Introduction

Due to their low density, magnesium and its alloys are distinguished by their high specific stiffness and strength, although they concomitantly exhibit outstanding biocompatibility, biodegradability and damping characteristics [1–5]. Nevertheless, their structural applications are limited by their low strength at ambient to elevated temperatures, especially when compared to other widely used metallic structural materials such as steels and aluminum alloys [6–8]. A feasible strengthening approach is to introduce reinforcement phases into the magnesium matrix to form magnesium composites [9–14]. The spatial characteristics of these reinforcements, however, can play a key role in governing the mechanical properties of the resulting composites. In this regard, generally major efforts have been devoted to achieve a uniform distribution of reinforcements within the magnesium matrix [9,10,15–17]. This tends to lead to a limited strengthening efficiency of rein-

* Corresponding author at: Institute of Metal Research, Chinese Academy of Sciences, Shenyang 110016, China.
** Corresponding author.
E-mail addresses: zengqianliu@imr.ac.cn (Z. Liu), mfqwang@cmu.edu.cn (Q. Wang).

https://doi.org/10.1016/j.jma.2021.06.023

Please cite this article as: Y. Liu, Q. Yu, G. Tan et al., Bioinspired fish-scale-like magnesium composites strengthened by contextures of continuous titanium fibers: Lessons from nature, Journal of Magnesium and Alloys, https://doi.org/10.1016/j.jma.2021.06.023

forcements because of their poor continuity, coupled with the lack of preferred orientation or alignment in the composites. Additionally, it is difficult with such conventional protocols to avoid a reduction in ductility while increasing the strength [9,15,18–20]. In this context, it is important to explore new architectural designs for improving the mechanical properties of magnesium alloys and their composites, especially from the perspective of seeking new strategies toward synergetic enhancement of both strength and ductility.

The lessons from Nature have been increasingly utilized in exploiting new high-performance structural materials [21–23]. Despite being composed of simple constituents, natural biological materials are particularly successful in developing remarkable mechanical properties, which can be comparable, or even superior, to those of the synthetic counterparts due to their delicate and complex architectures [24–27]. A good example is the fish scale which provides effective protection to fish without restraining their flexibility for motion [28–32]. In addition to the scale's hard outer layer which acts to resist penetration, the tougher base component underneath, which consists principally of lamellae of mineralized collagen fibers in non-collagenous matrix and comprises the major part of the scale, plays an important role in accommodating any excessive deformation to maintain the protective functionality of the scale [28,32–34].

Two representative types of architectures that have been identified in fish scales are the orthogonal plywood and Bouligand-type structures. The orthogonal plywood architecture consists of a mutually perpendicular alignment of collagen fibers between adjacent lamellae. It exists in the scales of different species of fish such as *Morone saxatilis* and *Pagrus major* [29,34]. The Bouligand-type architecture, conversely, exhibits a helicoidally twisting arrangement of collagen fibers which are rotated by a fixed angle between lamellae. Such an architecture is found in the scales of *Arapaima gigas* and *Cyprinus carpio* fish, and is capable of allowing the reorientation of the fibers adaptively under external load, which is a particularly effective mechanism for toughening the scale [28,31]. A unique variety of this Bouligand-type architecture has been identified in the scales of a "living fossil" coelacanth fish *Latimeria chalumnae* where the twisting units are composed of orthogonal bilayers comprising mutually perpendicular collagen fibers instead of unidirectional ones [31]. This structure, which has been described as the double-Bouligand architecture, appears to be more effective in enhancing the fracture toughness of materials than the more common single Bouligand-type architecture [31,35]. The exceptional mechanical efficiency of the double-Bouligand architecture can be explicitly verified by the fact that the coelacanth fish can survive in shark-infested waters.

Based on this inspiration from Nature, the hypothesis here is that the ingenious architectures of such fish scales may serve as ideal prototypes for designing new magnesium composites. Specifically, a strategy is proposed in this study for developing fish-scale-like magnesium composites which encompasses architectural design, selection of reinforcement phase, and employment of appropriate fabrication methods. First, the orthogonal plywood and double-Bouligand architectures of fish scales are replicated in magnesium composites by controlling the spatial arrangement of reinforcements. Second, titanium is selected as the reinforcement phase in view of its low density, good biocompatibility, and the absence of reactions or large solubility with the magnesium melt [36–39]. Third, the composites are fabricated by infiltrating the magnesium melt into contextures of continuous titanium fibers which utilizes the large difference between the melting points of titanium and magnesium along with the good wettability between them (Fig. 1). This study offers "proof of concept" in terms of the fabrication and microstructures of bioinspired magnesium composites as well as their mechanical properties at ambient to elevated temperatures under quasi-static and dynamic loading conditions. It shows how the salient mechanisms which induce the unique properties of fish scales can be implemented in a metal system and how the strength of resulting composites can be optimized by tailoring their architectural characteristics. This study may aid in the design of new bioinspired magnesium composites and other materials mimicking fish scales toward enhanced performance.

2. Experimental section

2.1. Architectural construction

Commercially available titanium meshes (Anheng Co., China) were chosen as the structural units for constructing bioinspired fish-scale-like architectures. These meshes are composed of continuous fibers of pure titanium which are perpendicularly interwoven together, as shown in Fig. 1. The diameter and interspacing of these fibers are ~70 μm and ~100 μm, respectively. The titanium meshes were cut into circular pieces with a diameter of 75 mm using scissors, and then ultrasonically cleaned successively with 1 wt.% oxalic acid in ethanol for 5 min and with pure ethanol to remove possible surface contaminants. These pieces were stacked layer-by-layer following different configurations for constructing the bioinspired orthogonal plywood and double-Bouligand architectures. Specifically, the alignments of titanium meshes were all consistent between layers for the orthogonal plywood architecture. For the double-Bouligand architecture, the meshes were twisted in right-handed fashion with a pitch angle of 7.5° between adjacent layers from bottom to up. It has been revealed that a small twisting angle, generally less than 10°, is preferred for enhanced damage tolerance in Bouligand-type structures [40–42]; however, it may lead to increased thickness for each cycle of the helix and thereby to obvious heterogeneities. Here the twisting angle was determined as 7.5° such that two complete cycles of helices can be generated in a lab-sized sample with a thickness of ~2.5 mm, *i.e.*, a total of 24 layers of titanium meshes are contained. The stacked pieces were then fixed at their periphery using stainless steel wires and densified by pressing along the thickness direction at 35 MPa for 2 h.

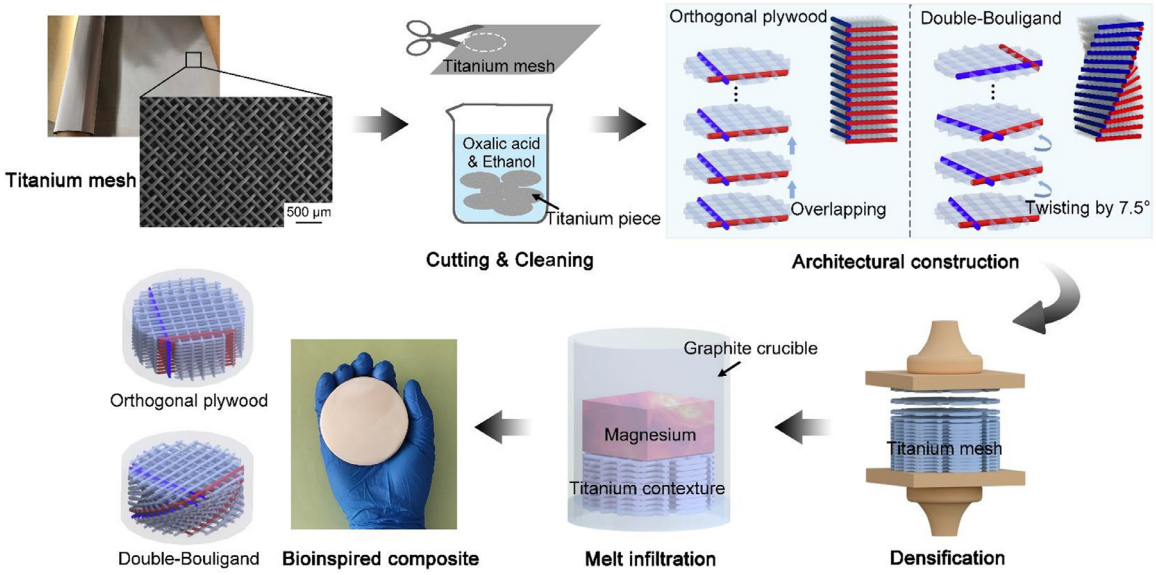

Fig. 1. Fabrication procedure of the bioinspired fish-scale-like magnesium composites strengthened with contextures of continuous titanium fibers.

2.2. Composite fabrication

Bioinspired magnesium composites were fabricated through pressureless infiltration of a magnesium melt into the contextures of stacked titanium meshes. The contextures were placed in high-purity graphite crucibles smeared with boron nitride paste. Blocks of pure magnesium were mechanically burnished to remove surface oxides and placed on top of the contextures. They were heated in flowing argon gas to 850 °C, *i.e.*, some 200 °C higher than the melting point of magnesium, held for 10 min, and then cooled in the furnace. Pure magnesium, solidified following the same procedure, and commercially available coarse-grained pure titanium were used as comparison materials.

2.3. Microstructural characterization

Scanning electron microscopy (SEM) imaging was performed using a LEO Supra-35 filed-emission scanning electron microscope (LEO, Germany) operating at an accelerating voltage of 20 kV. For microstructural observation, the infiltrated composites were sectioned across their thickness profile with the cutting direction parallel to one set of the orthogonal fibers at the top and bottom layers of the titanium meshes. The samples were then ground and polished to a surface finish of ~0.5 μm prior to examination. X-ray energy dispersive spectroscopy (EDS) measurements were conducted using an Oxford Model 7426 spectrometer (Oxford Instruments, UK) equipped with a microscope. The Archimedes' method was used to determine the densities of the composites, ρ, according to $\rho = \frac{m_1\rho_0}{m_1-m_2}$, where m_1 and m_2 denote the weights of samples in air and in distilled water, respectively, and ρ_0 is the density of distilled water [43].

2.4. X-ray tomography

X-ray tomography (XRT) imaging was performed using an Xradia Versa XRM-500 three-dimensional (3-D) X-ray microscope (Xradia, USA) operating at an accelerating voltage of 80 kV. A total of 1600 two-dimensional (2-D) projections were acquired for each sample by rotating it by 360° around the normal axis of the X-ray source and detector. 3-D volume renderings were reconstructed by inversing these projections based on the Fourier back-projection algorithm. The spatial resolution of the 3-D images was ~5 μm per pixel. Image processing and analysis were conducted using the Avizo Fire 7.1 software (Visualization Sciences Group, France). XRT imaging was also employed to quantify the changes in fiber orientations in the fractured samples from the tensile tests. The measurement was performed on the gauge sections with a uniform deformation, *i.e.*, between the fracture profile and the transition arc of the tensile specimen, which had a length of ~10 mm. At least 10 fibers were examined for a fixed initial orientation with the data presented in form of mean ± standard deviation.

2.5. Quasi-static tensile tests

Uniaxial tensile tests were conducted at both room temperature and 200 °C at a strain rate of 10^{-3} s^{-1} using an Instron 5982 testing system (Instron Co., USA). The samples had a gauge dimension of 13.5 mm × 6 mm × 2.6 mm and were ground and polished to a surface finish of ~0.5 μm before testing. Over 20 layers of titanium meshes were contained in all these samples throughout their thickness direction. This ensured the involvement of nearly two complete cycles of helices for the double-Bouligand architecture. Specifically, the loading direction conformed well to the alignment of one set

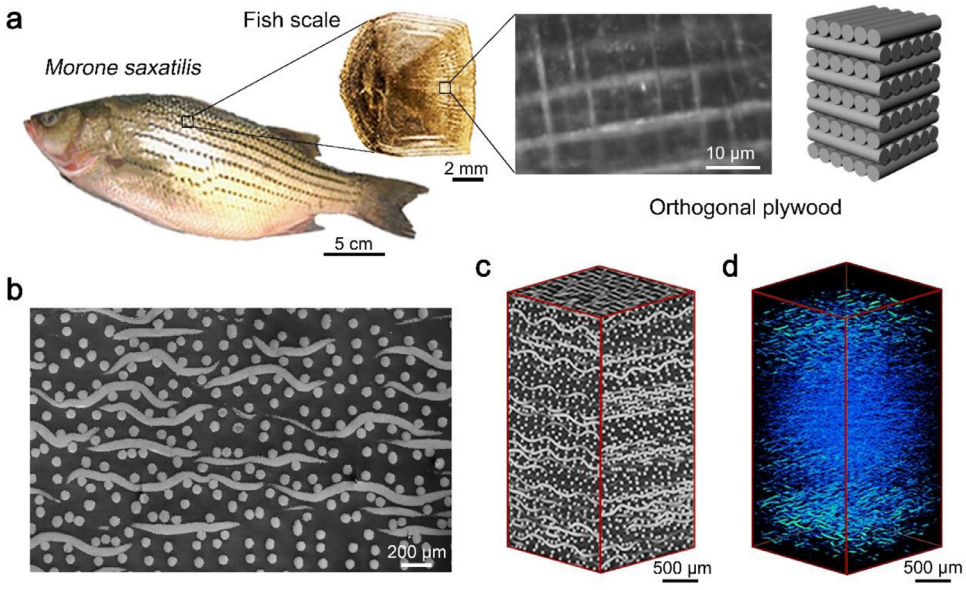

Fig. 2. Microstructure of magnesium composite with bioinspired fish-scale-like orthogonal plywood architecture. (a) Representative morphology and schematic illustration of the orthogonal plywood architecture in the scale of *Morone saxatilis* fish [29]. (b) Through-thickness SEM micrograph and (c, d) XRT volume renderings of the magnesium composite with bioinspired orthogonal plywood architecture. (d) shows the spatial arrangement of titanium fibers in the composite by filtering out the signal from magnesium matrix. The micrograph of fish scale in (a) is adapted with permission from Ref. [29].

of titanium fibers for the orthogonal plywood architecture. At least three measurements were conducted for each set of samples with the results presented in form of mean ± standard deviation.

2.6. Digital image correlation measurements

The strain distribution on the through-thickness lateral surfaces of samples during room temperature tensile tests was monitored using the digital image correlation (DIC) method. The DIC imaging was performed using an AVE 2 video extensometer (Instron Co., USA) equipped with an Instron 8862 testing machine (Instron Co., USA). Before measurement, the surfaces of samples were covered with black paint and then sprayed with contrasting white speckle patterns as strain markers.

2.7. Split Hopkinson pressure bar tests

Split Hopkinson pressure bar (SHPB) tests were performed at room temperature on cylindrical samples with a diameter of ∼7 mm and a thickness of ∼3 mm. In the SHPB tests, a striker bar was launched at a specific velocity against an incident bar which was attached successively to the sample, a transmitted bar and an absorbing bar. All the bars had an identical diameter of 15.5 mm and were made of steel characterized by a density of 7.8 g/cm^3 with an elastic modulus of 210 GPa. The impact load was along the thickness direction of samples which was perpendicular to the stacked titanium meshes. Before testing, the end surfaces of samples and incident bar were lubricated with silicone to reduce friction. The impact velocity of the striker bar was determined using a laser velocimeter (Jinggong Instrument Co., China). The small deformations of the incident and transmitted bars were captured by strain gauges attached to them; the measured strains were converted to electrical signals using a LK2107B high dynamic strain indicator (Longke Co., China). Stress-strain relationships were obtained from these signals by adopting a two-wave method [44,45].

3. Results

3.1. Fish-scale-like architectures

Fig. 1 shows a schematic illustration of the fabrication procedure for the bioinspired fish-scale-like magnesium composites and the overall appearance of the final products. The microstructures of composites and their comparisons with representative natural prototypes of fish scales are presented in Figs. 2 and 3. It is seen that the woven contextures of titanium fibers can be completely filled with magnesium through the pressureless infiltration technique. The spatial arrangements of titanium fibers within the composites can be clearly revealed by the through-thickness SEM micrographs and 3-D XRT volume renderings. The composites exhibit distinctly different fiber arrangements in line with the orthogonal plywood and double-Bouligand configurations, *i.e.*, the mutually perpendicular fibers demonstrate constant orientations for the former but are helicoidally twisted for the latter. Such characteristics are largely reminiscent of those of corresponding fish scales, *e.g.*, for *Morone saxatilis* and *Latimeria chalumnae* specifies respectively [29,31]. This indicates an effective implementation of bioinspired designs in the composites by regulating the stacking modes of titanium meshes. These architectures in the bioinspired composites are also similar to many other biological materials, such as the conch shell and the shell of

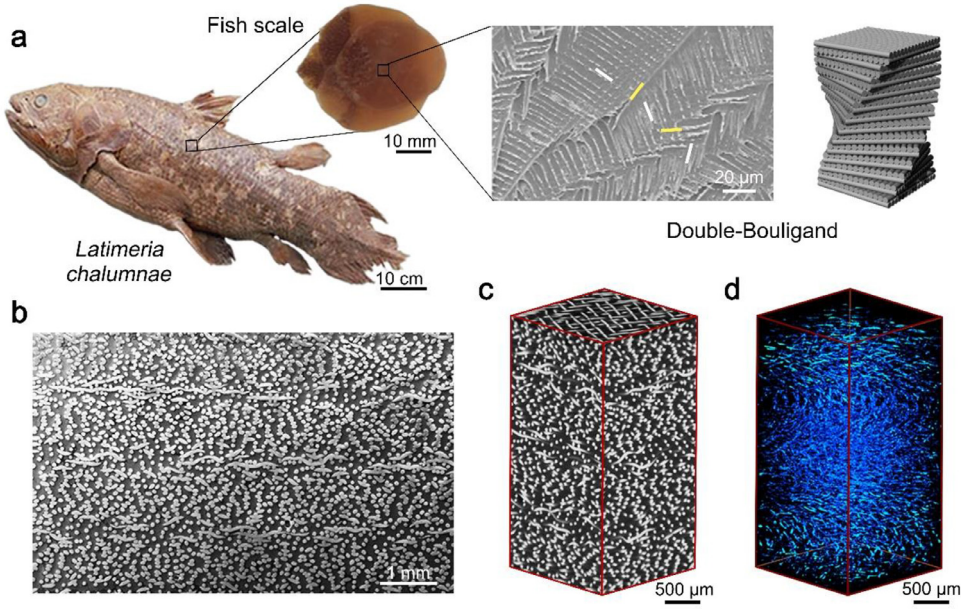

Fig. 3. Microstructure of magnesium composite with bioinspired fish-scale-like double-Bouligand architecture. (a) Morphology and schematic illustration of the double-Bouligand architecture in the scale of *Latimeria chalumnae* fish [31]. The white and yellow lines indicate the mineralized collagen fibers in twisting units which are mutually perpendicular. (b) SEM micrograph and (c, d) XRT volume renderings of the magnesium composite with bioinspired double-Bouligand architecture. (d) shows the spatial arrangement of titanium fibers in the composite. The micrograph of fish scale in (a) is adapted with permission from Ref. [31]. (For interpretation of the references to color in this figure legend, the reader is referred to the web version of this article.).

Pectinidae [46–49], in terms of the layered arrangement of their structural units and the variations in their orientation.

The volume fractions of titanium phase were measured by XRT to be ~33.0% and ~35.7%, respectively for the orthogonal plywood and double-Bouligand architectures. Accordingly, their densities can be calculated following the rule-of-mixtures as ~2.65 g/cm^3 and ~2.73 g/cm^3. These conform well to the experimentally measured values of 2.67 g/cm^3 and 2.71 g/cm^3, implying the absence of large voids in the composites and therefore the complete filling of the contextures by magnesium.

Despite the above similarities, a feature that makes the bioinspired composites distinctive from natural fish scales is that the reinforcing fibers are interwoven together within each lamina in the composites, instead of being comprised of two separate sublayers of unidirectional fibers as in fish scales [29,31–33]. It is expected that such a characteristic may promote an enhanced fracture resistance in the composites by hindering the separation between fibers. Indeed, this is also reminiscent of the fact that in fish scales the sublayers of unidirectional fibers are bonded together by inter-layer fibrils [31,50].

Fig. 4a and b show the magnified SEM images of the interfacial region between titanium and magnesium phases along with the distributions of elements across interface in the composites. It is seen that a small volume fraction of micrometer-sized titanium precipitations formed in the magnesium matrix. The magnesium content displays a gradual gradient in a range of over 10 μm across the phase interface, indicating that magnesium denudes the matrix across the interface by diffusing into the titanium phase. Nevertheless, the depletion of titanium content was principally limited within the interior of titanium phase in the vicinity behind the interface. Such characteristics originate essentially from the following two aspects: (i) atomic diffusion in magnesium melt is much faster than that in solid-state titanium during the melt infiltration process, which leads to the dissolution of titanium atoms into the magnesium melt, but only from the surface layer of titanium phase; (ii) the solid solubility of titanium in magnesium is minimal and obviously decreases with decreasing temperature [51]. As such, the dissolved titanium atoms were precipitated from magnesium matrix during the cooling process. These mechanisms are schematically depicted in Fig. 4c.

3.2. Quasi-static tensile properties

Fig. 5a and b show the engineering tensile stress-strain curves of the bioinspired fish-scale-like magnesium composites tested at room temperature and 200 °C. The results for individual constituents of pure magnesium and titanium are also presented for comparison (the data for pure titanium are shown in Fig. S1 in Supplementary Materials). The composites can be continuously work hardened at both temperatures after yielding, leading to uniform deformation without obvious necking until fracture, as indicated by the true stress-strain curves and work-hardening rate shown in Fig. 5c and d. The ultimate tensile strengths of the composites are markedly higher than those predicted from components according to the rule-of-mixtures, as indicated by the dashed curves (Fig. 5a and b). Specifically, the double-Bouligand architecture tends to exhibit further increases in strength and ductility, as com-

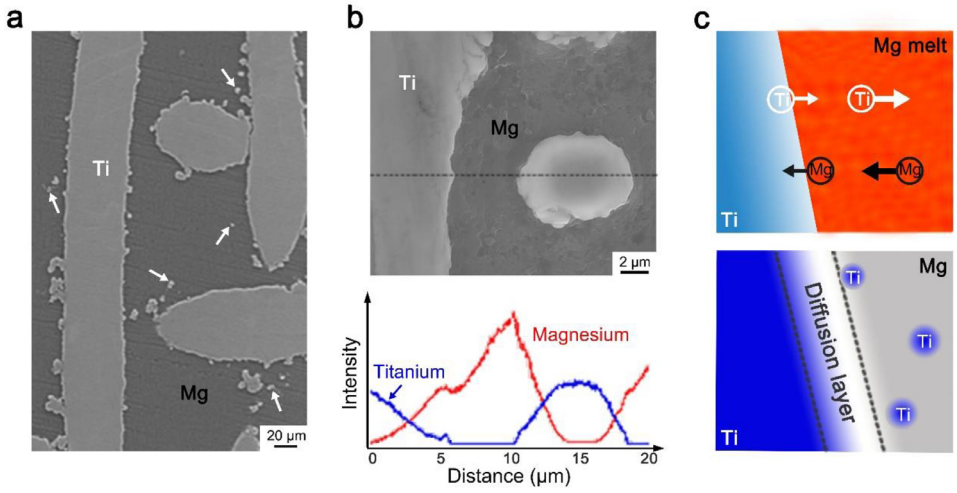

Fig. 4. Microstructural and chemical characteristics of the interfacial region between titanium and magnesium phases. (a) SEM micrograph showing the presence of titanium (Ti) precipitation in the magnesium (Mg) matrix, as indicated by the white arrows. (b) Magnified SEM micrograph and corresponding EDS line-scan results of the distribution of the titanium and magnesium elements across the interface between titanium and magnesium phases. (c) Schematic illustrations of the atomic diffusion of elements and titanium phase precipitation during the melt infiltration and cooling processes.

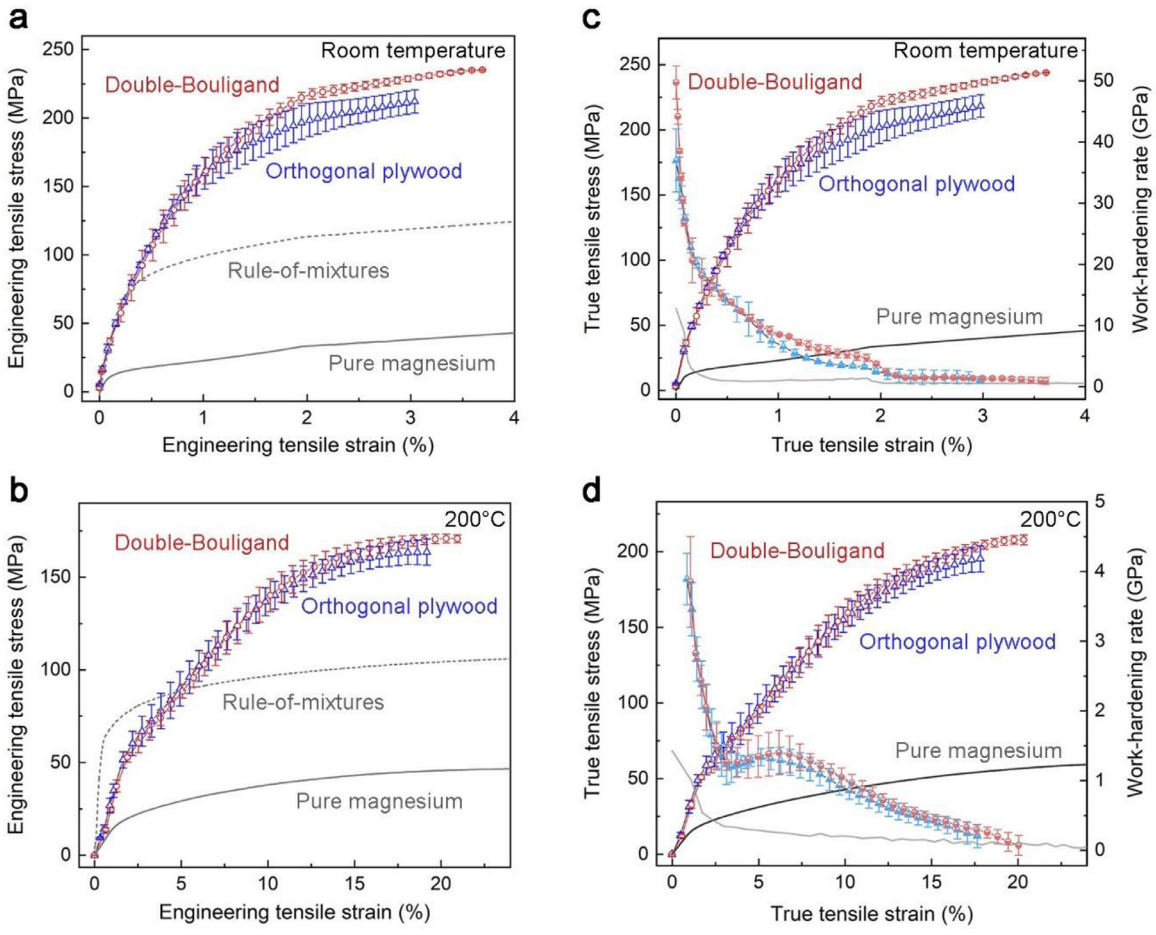

Fig. 5. Quasi-static tensile properties of the bioinspired fish-scale-like magnesium composites. (a, b) Engineering tensile stress-strain curves of the magnesium composites with bioinspired orthogonal plywood and double-Bouligand architectures at (a) room temperature and (b) 200 °C. Results for pure magnesium and approximations according to the rule-of-mixtures are also shown for comparison. (c, d) Variations in the true tensile stress (dark color) and work-hardening rate (light color) with the true tensile strain at (c) room temperature and (d) 200 °C for the magnesium composites as compared to pure magnesium.

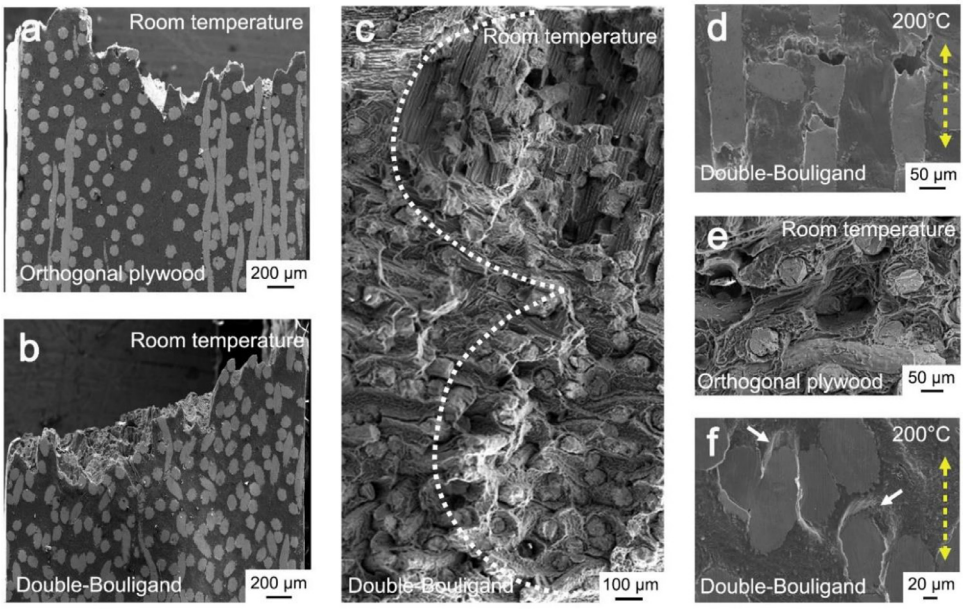

Fig. 6. Representative damage morphologies of the bioinspired magnesium composites after tensile testing. Fracture surfaces of the composites with the (a) orthogonal plywood and (b) double-Bouligand architectures. (c) Through-thickness SEM micrograph showing periodically helicoidal patterns, as indicated by the dashed curves, on the fracture profile of the composites with double-Bouligand architecture. Magnified SEM images showing the (d) rupture and (e) separation of titanium fibers which are parallel and perpendicular to the tensile axis, respectively, and the (f) interfacial slip of obliquely aligned fibers within the magnesium matrix. The slip traces are indicated by the white arrows in (f). The loading directions in (d) and (f) are indicated by the yellow dashed lines. (For interpretation of the references to color in this figure legend, the reader is referred to the web version of this article.)

pared to the orthogonal plywood architecture, at both room temperature and 200 °C, implying a higher mechanical efficiency. In contrast to the behavior at room temperature, a notable improvement in tensile ductility, although accompanied by an obvious decrease in strength, was observed at 200 °C for both architectures. This is caused by the easy slippage between titanium fibers within the magnesium matrix because of the latter's creep behavior (as will be shown below in Fig. 6) [52].

It should be noted here that the current bioinspired composites are inferior to many other magnesium composites and alloys in terms of their absolute mechanical properties [13,20,53]. This is because of the use of simple pure elements as constituents, *i.e.*, pure magnesium and titanium, and the fact that coarse grains are formed in them during the slow solidification and cooling processes; this was deliberately done to help discern the effects of the bioinspired architectures by excluding other confusing factors. However, the chemical and microstructural characteristics of the components used to make these magnesium composites can be readily tuned to achieve enhanced properties in the materials.

As shown in Fig. 6, the tensile fracture surfaces of the bioinspired composites demonstrate a large tortuosity depending on the orientations of titanium fibers. Specifically, the composite with the double-Bouligand architecture displays periodically helicoidal patterns on fracture profiles, conforming exactly to the arrangement of titanium fibers (Fig. 6c). At both temperatures, the fibers that are parallel to the tensile axis are ruptured (Fig. 6d), although they are separated from each other in the case of perpendicular configuration (Fig. 6e). The obliquely aligned fibers tend to be tilted within the magnesium matrix through interfacial slippage, as clearly manifested by the slip traces indicated by the white arrows (Fig. 6f), thereby deviating from their original orientations. Such a trend becomes much more evident at elevated temperature owing to the creep behavior of the magnesium. The fish-scale-like architectures have been replicated in a variety of non-metallic materials where the reinforcing fibers are brittle [40,41,54]. In contrast, the titanium fibers in the current composites are deformable under the applied tensile load, which qualitatively resembles the case found in fish scales and also in the conch shell [29–31,33,34,55]. DIC images of the through-thickness surfaces of the tensile samples, shown in Fig. 7, reveal a good conformity of local strain distributions with fiber arrangements in the composites. Specifically, relatively high strains are concentrated at nearly flat sections for the orthogonal plywood architecture, but demonstrate a broader distribution in helical-shaped areas for the double-Bouligand architecture, suggesting a more effective role of the latter structure in mitigating strain localization. The DIC results for the entire deformation processes of the composites with the two architectures are shown in Supplementary Movies S1 and S2.

3.3. Dynamic mechanical properties

Fig. 8a shows representative high strain-rate stress-strain curves of the bioinspired composites as compared to pure magnesium under SHPB impact loading at a comparable impact velocity of ∼11 m/s. The variations in the peak stress

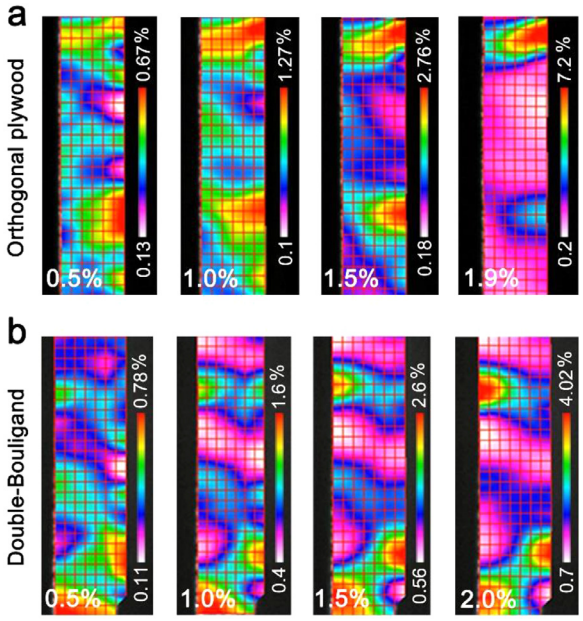

Fig. 7. Successive DIC images of through-thickness surfaces showing the local strain distributions in the magnesium composites with bioinspired (a) orthogonal plywood and (b) double-Bouligand architectures after loading to incremental strains during tensile tests at room temperature.

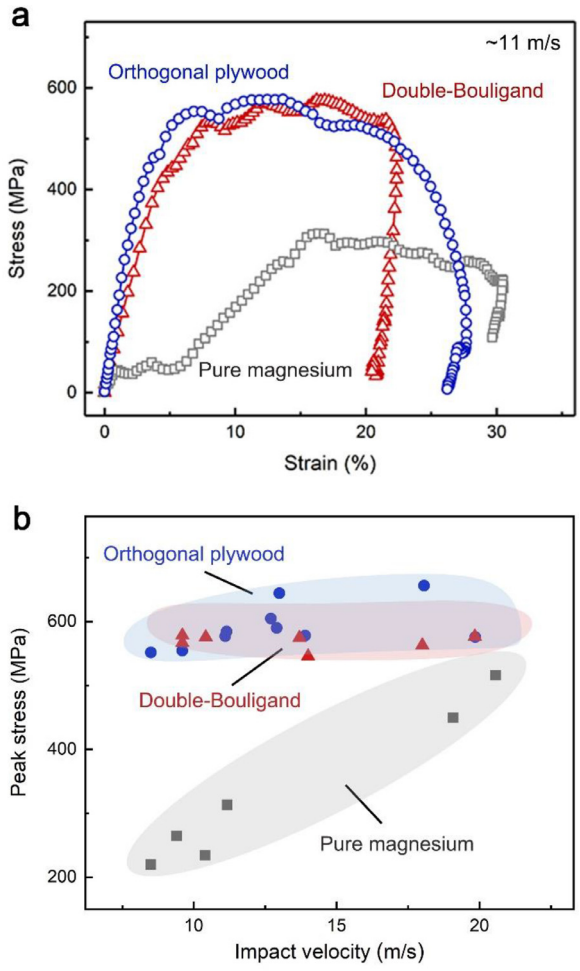

Fig. 8. Dynamic mechanical properties of the bioinspired fish-scale-like magnesium composites. (a) Representative stress-strain curves of the magnesium composites with bioinspired orthogonal plywood and double-Bouligand architectures as compared to pure magnesium under SHPB impact loading at a comparable impact velocity of ~11 m/s. (b) Variations in peak stress with impact velocity for the composites and constituent materials.

with impact velocity are presented in Fig. 8b. The stress-strain curves of the composites are characterized by a relatively stable stress plateau with the peak stresses markedly exceeding the quasi-static strengths and those of pure magnesium. The peak stresses of the composites remain nearly constant at around 600 MPa in the experimental ranges of impact velocity from ~8 m/s to ~20 m/s. By contrast, pure magnesium displays a clear rising trend of peak stress with increasing impact velocity. Additionally, the composites with the bioinspired orthogonal plywood and double-Bouligand architectures exhibit comparable peak stresses at different impact velocities, implying a minimal dependence of dynamic mechanical properties on the fiber alignments.

The overall appearance and representative fracture morphologies of the bioinspired composites after SHPB tests are shown in Fig. 9. The composites exhibit increasingly larger deformation as the impact velocity increases (Fig. 9a). The failure of the composites with either architecture is dominated by a mode of shear fracture along primary shear bands as indicated by the white arrows. The shear bands can easily penetrate the fibers regardless of their stacking configurations. This further implies a limited effect of architectures on the impact behavior of the composites. Rupture of the titanium fibers is evident as can be seen from the impact surfaces of samples (Fig. 9b), especially at the intersections between mutually perpendicular fibers where stress concentrations are generated. Additionally, distinct from the apparent melting on the fracture profiles for pure magnesium (Fig. S2), local melting only occurred near the impact faces in the composites (Fig. 9c), conforming well to their improved impact resistance.

3.4. Adaptive structural reorientation characteristics

Fig. 10a shows the 3-D arrangements of titanium fibers in the composites with the double-Bouligand architecture after tensile tests at room and elevated temperatures, as revealed by XRT. The orientations of fibers in each lamina with different alignments can be clearly illuminated by serially dissecting the 3-D images along their basal planes, with representative 2-D slices shown in Fig. 10b. Here the initial orientations of these fibers were determined from the undeformed grip sections using the same methods. It can be seen that the grids of titanium meshes are clearly distorted from their original square shape (Figs. 10b and S3), indicating the changes in fiber orientations during the deformation process. A general trend is that most of the fibers tend to rotate towards the tensile direction, leading to a decrease of their inclination angle with respect to the loading axis. This closely resembles the adaptive structural reorientation behavior of fish scales

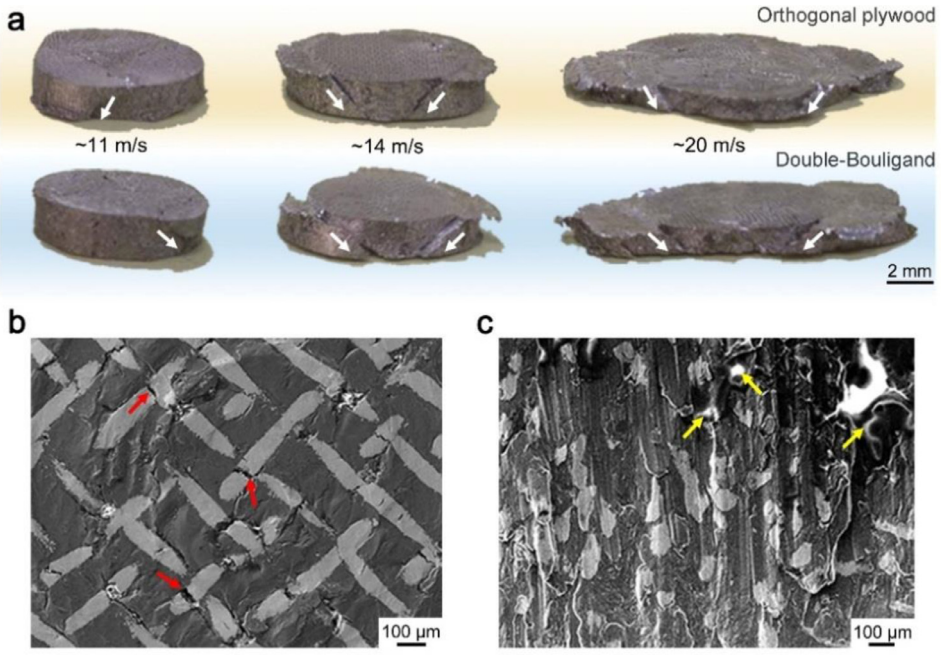

Fig. 9. Representative damage morphologies of the bioinspired magnesium composites after impact loading. (a) Overall appearance of the composites after SHPB tests loaded at different impact velocities. The dominant shear bands are indicated by the white arrows. SEM micrographs of the (b) impact surface and (c) fracture profile of the composites showing the rupture of titanium fibers and local melting of magnesium matrix, as indicated by the red and yellow arrows respectively. (For interpretation of the references to color in this figure legend, the reader is referred to the web version of this article.)

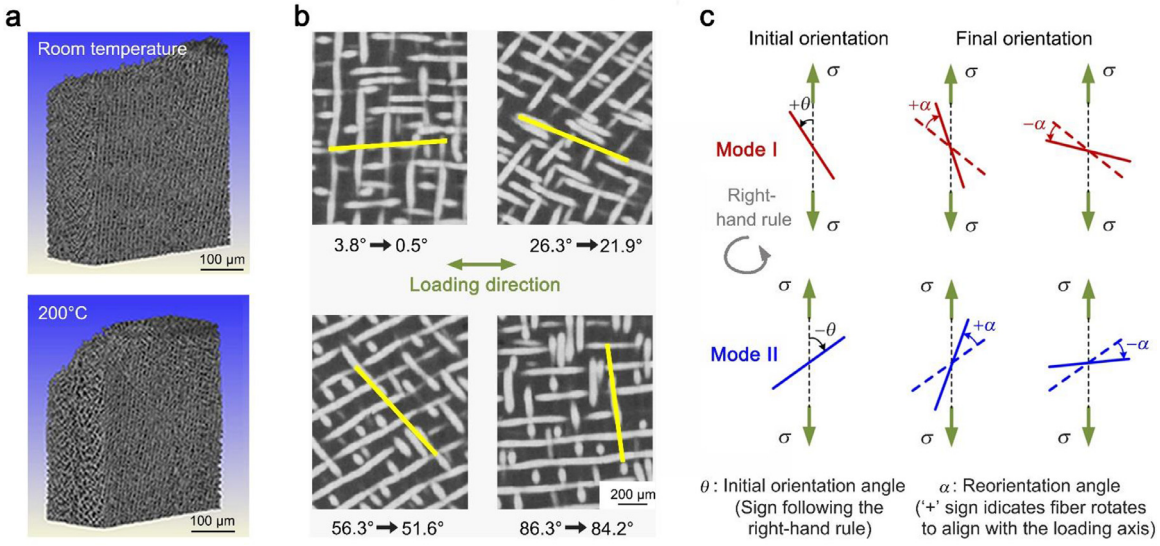

Fig. 10. Adaptive structural reorientation behavior of titanium fibers in the bioinspired magnesium composites with the double-Bouligand architecture. (a) XRT volume renderings of fractured samples showing the spatial arrangement of the titanium fibers in the composites after tensile tests at room temperature and 200 °C. (b) 2-D slices of an XRT image showing the alignment of titanium fibers with different initial orientations in the composites after tensile testing at 200 °C. The initial and final orientations for a set of fibers (marked as yellow) with respect to the loading direction are indicated in the figure. (c) Schematic illustrations of the two modes for the initial orientations of the titanium fibers and their corresponding reorientations. (For interpretation of the references to color in this figure legend, the reader is referred to the web version of this article.)

where the majority of the fibers rotate towards the loading direction to carry more load [30,31,56,57].

Here the reorientation angles of fibers, *i.e.*, the differences between their final and initial orientations, are defined to be positive in the above fashion and negative when the fibers are deviated away from the loading axis, as illustrated in Fig. 10c. The varying shape changes of grids, shown in Figs. 10b and S3, suggest that the reorientation of fibers is dependent on their initial orientations. Specifically, the reorientation direction may be contrary to, or consistent with, the twisting direction between fiber meshes according to the right-hand rule (Fig. 10c). To facilitate the discussion, the initial orientations

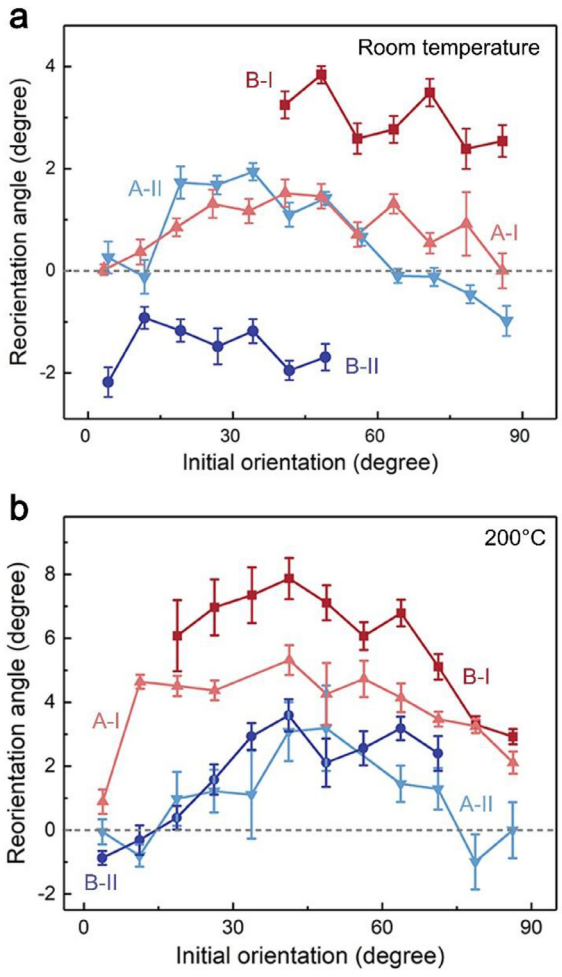

Fig. 11. Variations in the reorientation angles of titanium fibers as a function of their initial orientations in the bioinspired magnesium composites with the double-Bouligand architecture after tensile tests at (a) room temperature and (b) 200 °C. A and B indicate the two twisting helices of fibers involved in the composite. I and II represent the two modes of the initial fiber orientations.

of fibers that are positive and negative with respect to the loading axis (following the right-hand rule) are referred to as mode I and mode II, respectively (Fig. 10c).

The detailed variations in reorientation angles of fibers as a function of their initial orientations are presented in Fig. 11. Here the initial orientation angles with respect to the loading axis, which are positive and negative respectively for mode I and II initial orientations (Fig. 10c), are represented using their absolute values on the x axis. It is seen that the reorientation of titanium fibers becomes considerably more evident at 200 °C as compared to room temperature because of the easy creep deformation of magnesium matrix. At both temperatures, the reorientation angles display an initially increasing trend and then decrease with the increase of initial orientations. The most significant reorientation is generated when the fibers are initially aligned at around 45° with respect to the loading axis, conforming well to the plane with the maximum resolved shear stress. This is consistent with observations in fish scales where reorientation was found to be more evident for obliquely aligned fibers [30,31]. In addition, with regard to fibers within the same twisting helix (indicated by A or B in Fig. 11), the mode II initial orientation tends to display a larger resistance than mode I, as manifested by its smaller reorientation angles. In particular, the reorientation angles may even become negative for the mode II initial orientation, especially when the initial orientations of fibers approach 0° or 90° This means that the fibers which are nearly parallel or perpendicular to the loading axis may rotate away from the tensile direction. A similar phenomenon has been detected in fish scales and has been attributed to the local compressive stresses at such configurations [30,31].

4. Discussion

Classical laminate theory [58] is modified here for the bioinspired Bouligand-type architectures to interpret their room-temperature tensile properties. The composite model, as illustrated in Fig. 12a, consists of 24 layers of laminae with each comprising a bilayer of orthogonal fibers. These laminae, numbered by k^{th} (k = 1, 2, …, 24), are sequentially stacked from the bottom up following an anticlockwise spiral fashion with a pitch angle φ. The upper and lower laminae at an equal Z-distance from the middle plane display antisymmetric configurations in the composite. These structural characteristics are all in line with those in the experiments. The length and width of the model are set as unity. The local coordinate system for each individual lamina (1, 2) is consistent with the axial directions of the orthogonal fibers. The global coordinate system of the entire laminate composite is described by (X, Y, Z). Here the principal axes X and Y are defined using the bisectors of local principal axes of the 12$^{\text{th}}$ and 13$^{\text{th}}$ laminae, *i.e.*, the middle plane of the system. Both local and global coordinate systems are right-handed.

When applying a load along the loading axis L_1, which conforms to the principal axis of the 1$^{\text{st}}$ lamina here, the principal forces $\boldsymbol{\sigma}$ and moments $\boldsymbol{m}$ of the laminate normalized by the area or equivalently thickness of the model can be described as:

$$\begin{bmatrix} \boldsymbol{\sigma} \\ \boldsymbol{m} \end{bmatrix} = \begin{bmatrix} \boldsymbol{A} & \boldsymbol{B} \\ \boldsymbol{B} & \boldsymbol{D} \end{bmatrix} \begin{bmatrix} \boldsymbol{\varepsilon_0} \\ \boldsymbol{\kappa} \end{bmatrix}, \tag{1}$$

with $\boldsymbol{\varepsilon_0}$ and $\boldsymbol{\kappa}$ denoting the plane strains and curvatures [59,60]. The parameters $\boldsymbol{A}$, $\boldsymbol{B}$ and $\boldsymbol{D}$ are stiffness matrices for the stress states of extension, extension-bending coupling and bending, respectively. All these variables and parameters are in vector form. The plane stress of the k^{th} lamina can be deduced to be:

$$\boldsymbol{\sigma}_{mk} = \boldsymbol{Q}_{1,2}\boldsymbol{T}_{\mathbf{k}}\boldsymbol{T}\boldsymbol{s}\boldsymbol{R}\sigma_{th} = \boldsymbol{P}_{\mathbf{k}}\sigma_{th}, \tag{2}$$

with $\boldsymbol{P_k} = \boldsymbol{Q}_{1,2}\boldsymbol{T_k}\boldsymbol{T}\boldsymbol{s}\boldsymbol{R}$ [58]. $\boldsymbol{\sigma}_{th}$ is the critical stress along the L_1 direction, and $\boldsymbol{T_k}$ and $\boldsymbol{T}$ are transformation matrices. $\boldsymbol{Q}_{1,2}$ and $\boldsymbol{s}$ are the lamina stiffness matrix in coordinate (1, 2) and the laminate compliance matrix in loading coordinate (L_1, L_2), respectively. The parameter $\boldsymbol{R}$ is described by $\boldsymbol{R} = [1 \quad i \quad j]^{\text{T}}$ where i and j are the ratios of the stress along L_2 direction and the shear stress in the (L_1, L_2) coordinate with

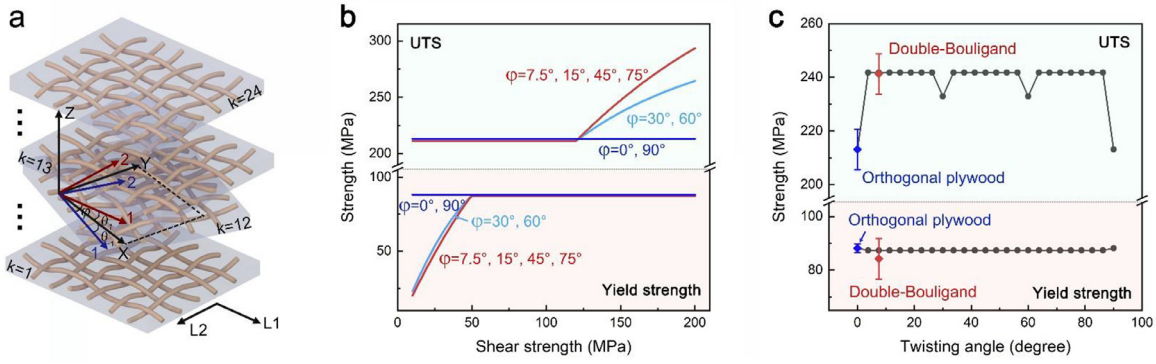

Fig. 12. Theoretical interpretation of the strengths for the magnesium composites with bioinspired orthogonal plywood and double-Bouligand architectures. (a) Schematic illustrations of the laminate composite model and coordinate system for the theoretical analysis. (b) Analytical results for the variation in yield and ultimate tensile (UTS) strengths of the laminate as a function of the shear strength of the lamina for the bioinspired orthogonal plywood and double-Bouligand architectures. The orthogonal plywood architecture can be seen as a unique double-Bouligand architecture with the twisting angle between the layers φ equal to 0° or 90°. (c) Theoretical and experimental results of the strengths for the bioinspired magnesium composites with different twisting angles between layers.

respect to σ_{th}. The detailed derivation processes are presented in the Supplementary Materials.

The Tsai-Hill failure criterion has demonstrated a good applicability in laminate composites reinforced with stiff fibers, including those with Bouligand-type architectures [60–62]. According to this criterion, the strength of the laminate along the L_1 direction can be eventually described as:

$$\sigma_{th} = \left(\frac{P_{k1}^2 - P_{k1}P_{k2}}{X^2} + \frac{P_{k2}^2}{Y^2} + \frac{P_{k12}^2}{S^2} \right)^{-\frac{1}{2}}, \tag{3}$$

where X and Y are the principal strengths along 1 and 2 axes in individual lamina, and S is the shear strength [59–62]. The 1 and 2 axes are equivalent in each lamina comprising orthogonal fibers, giving $X = Y$. The principal strengths of individual lamina can be approximated using those measured experimentally for the composite with the orthogonal plywood architecture. This is rationalized by the fact that the fiber alignments are all consistent among laminae in the composite. Then, the yield strength of laminate can be obtained by combining Eqs. (2) and (3) following the conservative first-ply failure criterion which assumes that the yielding of entire laminate is caused by the failure of the first lamina [63,64]. Similarly, the ultimate tensile strength of laminate can be approximated using the critical stress corresponding to the failure of the final lamina [65,66].

Fig. 12b presents the theoretical results of the variation in yield strength, *i.e.*, the stress corresponding to a plastic strain of 0.2%, and ultimate tensile strength for the bioinspired double-Bouligand architecture as a function of the shear strength of the lamina. The orthogonal plywood architecture can be seen as a unique double-Bouligand one where the twisting angle between layers, φ, equals 0° or 90° Here only specific twisting angles that are exactly divisible by 90° are considered to ensure the presence of full cycles of helices in the laminate. It is evident that the orthogonal plywood architecture ($\varphi = 0°$ or 90°) exhibits constant strengths over the wide range of shear strengths of the lamina. In contrast, the yield and ultimate tensile strengths of the double-Bouligand architecture ($\varphi \neq 0°$ or 90°) are largely dependent on the shear strength of the lamina, yet their varying trends are markedly different. Specifically, the yield strength initially increases and then remains constant with the increase of shear strength. The yield strength of the double-Bouligand architecture is invariably lower than that of the orthogonal plywood architecture. In comparison, the ultimate tensile strength of the double-Bouligand architecture initially remains constant and is slightly lower than that of orthogonal plywood architecture. It then displays a monotonic increasing trend as the shear strength of the lamina increases.

As shown in Fig. 12c, the strengths of the current composites can be well described based on the above analysis. The shear strength of lamina was fitted to be 145 MPa, *i.e.*, ~70% with respect to its ultimate tensile strength. This conforms to the empirical relationships where the shear strength of metals generally accounts for 60 to 80% of their ultimate tensile strengths [67,68]. The theoretical model reveals that the double-Bouligand architecture can effectively improve the ultimate tensile strength of the laminate composite while slightly decreasing its yield strength, thereby leading to an enhanced work-hardening capability. Such an effect is positively related to the shear strength of the lamina. Specifically, the shear failure of the lamina necessitates the rupture of fibers in the current composites because of the interwoven nature of the mutually perpendicular titanium fibers. This plays an effective role in improving the shear strength of the lamina. Additionally, with respect to the double-Bouligand architecture, the strengths remain nearly constant at varying twisting angles except for some decrease in the ultimate tensile strength at $\varphi = 30°$ or 60° Nevertheless, a small twisting angle will definitely promote better strain uniformity between adjacent laminae and is clearly favorable for enhanced fracture toughness through the deflection of cracks.

It is anticipated that the magnesium composites reinforced by continuous titanium contextures may serve as a new lightweight metallic material system for structural applications. In particular, their mechanical properties may be tai-

lored over a wide range by modulating the fish-scale-like architectures and controlling the content and chemical compositions of the constituents. In addition, these composites may be promising for biomedical applications. Specifically, both magnesium and titanium exhibit a good biocompatibility and have been extensively explored for biomedical use, *e.g.*, as bone substitute implants [36–38,69,70]. Nevertheless, they demonstrate completely different biodegradability with the magnesium and titanium being fully degradable and non-degradable, respectively. Indeed, magnesium-titanium composites may offer the possibility for exploiting new partially degradable biomedical materials. The gradual degradation of magnesium in composites may allow for the growth of new tissues into the titanium scaffolds or contextures, thereby achieving good tissue-implant integration. During the entire process, the titanium scaffolds could provide enough robustness to accomplish its mechanical function. Such concepts will be probed in future studies.

5. Conclusions

New magnesium composites strengthened by contextures of continuous titanium fibers were fabricated by pressureless infiltration of a magnesium melt into stacked titanium meshes. Bioinspired fish-scale-like orthogonal plywood and double-Bouligand architectures were constructed in the composites by controlling the fiber arrangements. These composites exhibit improved work-hardening ability and ultimate tensile strengths exceeding the rule-of-mixtures estimates from their constituents at ambient to elevated temperatures. The double-Bouligand architecture plays a more effective role than the orthogonal plywood one in mitigating strain localization and deflecting crack paths. In particular, the fibers in this architecture can adaptively reorient during the deformation process of composites by differing degrees depending on their initial orientations. This resembles to a large extent the adaptive structural reorientation behavior of fish scales, implying an implementation of the property-optimizing mechanisms behind the architecture. Composites with orthogonal plywood and double-Bouligand architectures demonstrate similar impact behavior with their peak stresses nearly independent of impact velocity. The strengths of the developed magnesium composites were interpreted by adapting classical laminate theory in line with their architectures. The double-Bouligand architecture was revealed to promote an improved ultimate tensile strength with a slight decrease in yield strength, which is associated with the shear strength of the lamina, thereby leading to enhanced work-hardening capability as compared to the orthogonal plywood architecture. The current fish-scale-like design concept and fabrication approach based on infiltration of a metal melt into fiber contextures with higher melting point may be extended to other material systems toward enhanced performance. The model and analysis could aid in guiding the architectural design and property optimization of these composites.

Declaration of Competing Interest

The authors declare no conflict of interest.

Data availability

The data that support the findings of this study are available from the corresponding author, Prof. Zengqian Liu, at zengqianliu@imr.ac.cn, upon reasonable request.

Acknowledgments

The authors are grateful for the financial support by the National Key R&D Program of China under grant number 2020YFA0710404, the National Natural Science Foundation of China under grant number 51871216, the KC Wong Education Foundation (GJTD-2020-09), the LiaoNing Revitalization Talents Program, the State Key Laboratory for Modification of Chemical Fibers and Polymer Materials at Donghua University, the Opening Project of Jiangsu Province Key Laboratory of High-End Structural Materials under grant number hsm1801, the Opening Project of National Key Laboratory of Shock Wave and Detonation Physics under grant number 6142A03203002, and the Youth Innovation Promotion Association CAS. ROR was supported by the Multi-University Research Initiative under grant number AFOSR-FA9550-15-1-0009 from the Air Force Office of Scientific Research.

References

[1] T.M. Pollock, Science 328 (2010) 986–987.
[2] F. Pan, M. Yang, X. Chen, J. Mater. Sci. Technol. 32 (2016) 1211–1221.
[3] R. Radha, D. Sreekanth, J. Magnes. Alloy. 5 (2017) 286–312.
[4] J. Song, J. She, D. Chen, F. Pan, J. Magnes. Alloy. 8 (2020) 1–41.
[5] Y. Zheng, X. Gu, F. Witte, Mater. Sci. Eng. R Rep. 77 (2014) 1–34.
[6] A. Luo, M. Pekguleryuz, J. Mater. Sci. 29 (1994) 5259–5271.
[7] B. Mordike, T. Ebert, Mater. Sci. Eng. A 302 (2001) 37–45.
[8] A.A. Luo, Int. Mater. Rev. 49 (2004) 13–30.
[9] D. Lloyd, Int. Mater. Rev. 39 (1994) 1–23.
[10] Q. Jiang, X. Li, H. Wang, Scr. Mater. 48 (2003) 713–717.
[11] X. Wang, D. Xu, R. Wu, X. Chen, Q. Peng, L. Jin, Y. Xin, Z. Zhang, Y. Liu, X. Chen, G. Chen, K. Deng, H. Wang, J. Mater. Sci. Technol. 34 (2018) 245–247.
[12] M. Habibnejad-Korayem, R. Mahmudi, W.J. Poole, Mater. Sci. Eng. A 519 (2009) 198–203.
[13] M.K. Habibi, S.P. Joshi, M. Gupta, Acta Mater. 58 (2010) 6104–6114.
[14] M. Zhang, Q. Yu, Z. Liu, J. Zhang, G. Tan, D. Jiao, W. Zhu, S. Li, Z. Zhang, R. Yang, Sci. Adv. 6 (2020) 5581.
[15] A. Luo, Metall. Mater. Trans. A 26 (1995) 2445–2455.
[16] S.F. Hassan, M. Gupta, J. Alloy. Compd. 345 (2002) 246–251.
[17] S. Hassan, M. Gupta, Mater. Sci. Eng. A 392 (2005) 163–168.
[18] H. Ferkel, B. Mordike, Mater. Sci. Eng. A 298 (2001) 193–199.
[19] S. Seshan, M. Jayamathy, S. Kailas, T.S. Srivatsan, Mater. Sci. Eng. A 363 (2003) 345–351.
[20] X. Zhong, W. Wong, M. Gupta, Acta Mater. 55 (2007) 6338–6344.
[21] G. Mayer, Science 310 (2005) 1144–1147.
[22] E. Munch, M.E. Launey, D.H. Alsem, E. Saiz, A.P. Tomsia, R.O. Ritchie, Science 322 (2008) 1516–1520.
[23] G. Tan, J. Zhang, L. Zheng, D. Jiao, Z. Liu, Z. Zhang, R.O. Ritchie, Adv. Mater. 31 (2019) 1904603.
[24] S. Ling, D.L. Kaplan, M.J. Buehler, Nat. Rev. Mater. 3 (2018) 1–15.
[25] U.G.K. Wegst, H. Bai, E. Saiz, A.P. Tomsia, R.O. Ritchie, Nat. Mater. 14 (2015) 23–36.

[26] Z. Liu, Z. Zhang, R.O. Ritchie, Adv. Mater. 30 (2018) 1705220.
[27] H.D. Espinosa, J.E. Rim, F. Barthelat, M.J. Buehler, Prog. Mater. Sci. 54 (2009) 1059–1100.
[28] Y. Lin, C. Wei, E. Olevsky, M.A. Meyers, J. Mech. Behav. Biomed. Mater. 4 (2011) 1145–1156.
[29] D. Zhu, C.F. Ortega, R. Motamedi, L. Szewciw, F. Vernerey, F. Barthelat, Adv. Eng. Mater. 14 (2012) B185–B194.
[30] E.A. Zimmermann, B. Gludovatz, E. Schaible, N.K. Dave, W. Yang, M.A. Meyers, R.O. Ritchie, Nat. Commun. 4 (2013) 1–7.
[31] H. Quan, W. Yang, E. Schaible, R.O. Ritchie, M.A. Meyers, Adv. Funct. Mater. 28 (2018) 1804237.
[32] M.M. Smith, M. Hobdell, W. Miller, J. Zool. 167 (1972) 501–509.
[33] A.K. Dastjerdi, F. Barthelat, J. Mech. Behav. Biomed. Mater. 52 (2015) 95–107.
[34] T. Ikoma, H. Kobayashi, J. Tanaka, D. Walsh, S. Mann, J. Struct. Biol. 142 (2003) 327–333.
[35] V.R. Sherman, H. Quan, W. Yang, R.O. Ritchie, M.A. Meyers, J. Mech. Behav. Biomed. Mater. 73 (2017) 1–16.
[36] M. Balog, A.M.H. Ibrahim, P. Krizik, O. Bajana, A. Klimova, A. Catic, Z. Schauperl, J. Mech. Behav. Biomed. Mater. 90 (2019) 45–53.
[37] S. Ouyang, Q. Huang, Y. Liu, Z. Ouyang, L. Liang, Bioact. Mater. 4 (2019) 37–42.
[38] S. Ouyang, Y. Liu, Q. Huang, Z. Gan, H. Tang, Mater. Sci. Eng. C 107 (2020) 110327.
[39] S. Jiang, L. Huang, Q. An, L. Geng, X. Wang, S. Wang, J. Mech. Behav. Biomed. Mater. 81 (2018) 10–15.
[40] L. Cheng, A. Thomas, J.L. Glancey, A.M. Karlsson, Compos. Part A 42 (2011) 211–220.
[41] J. Liu, H. Lee, V. Tan, Compos. Sci. Technol. 165 (2018) 282–289.
[42] Y. Zhang, G. Tan, M. Zhang, Q. Yu, Z. Liu, Y. Liu, J. Zhang, D. Jiao, F. Wang, L. Zhuo, Z. Zhang, R.O. Ritchie, J. Mater. Sci. Technol. 96 (2022) 21–30.
[43] S.W. Hughes, Phys. Educ. 40 (2005) 468–474.
[44] W. Chen, B. Song, D. Frew, M. Forrestal, Exp. Mech. 43 (2003) 20–23.
[45] L. Song, S. Hu, Explos. Shock Waves 25 (2005) 368.
[46] H. Li, X. Li, J. Bionic Eng. 16 (2019) 711–718.
[47] H. Li, J. Shen, Q. Wei, X. Li, Mater. Sci. Eng. C 103 (2019) 109820.
[48] H. Li, Z. Xu, X. Li, J. Struct. Biol. 184 (2013) 409–416.
[49] X. Li, P. Nardi, Nanotechnology 15 (2004) 211–217.
[50] M. Giraud, J. Castanet, F. Meunier, Y. Bouligand, Tissue Cell 10 (1978) 671–686.
[51] J. Murray, Alloy Phase Diagr. 7 (1986) 245–248.
[52] S.S. Vagarali, T.G. Langdon, Acta Metall. 29 (1981) 1969–1982.
[53] J. Koike, T. Kobayashi, T. Mukai, H. Watanabe, M. Suzuki, K. Maruyama, K. Higashi, Acta Mater. 51 (2003) 2055–2065.
[54] L.K. Grunenfelder, N. Suksangpanya, C. Salinas, G. Milliron, N. Yaraghi, S. Herrera, K. Evans-Lutterodt, S.R. Nutt, P. Zavattieri, D. Kisailus, Acta Biomater. 10 (2014) 3997–4008.
[55] H. Li, Y. Yue, X. Han, X. Li, Nano Lett. 14 (2014) 2578–2583.
[56] Z. Liu, Z. Zhang, R.O. Ritchie, Adv. Funct. Mater. 30 (2020) 1908121.
[57] Z. Liu, Y. Zhang, M. Zhang, G. Tan, Y. Zhu, Z. Zhang, R.O. Ritchie, Acta Biomater. 86 (2019) 96–108.
[58] R.M. Jones, Mechanics of Composite Materials, CRC Press, Philadelphia, USA, 2014.
[59] I. Greenfeld, I. Kellersztein, H.D. Wagner, Nat. Commun. 11 (2020) 1–12.
[60] R. Hill, J. Mech. Phys. Solids 12 (1964) 199–212.
[61] S.W. Tsai, in: R.T. Schwartz, H.S. Schwartz (Eds.), Fundamental Aspects of Fiber Reinforced Plastic Composites, Wiley, New York, 1968, pp. 3–11.
[62] S.W. Tsai, E.M. Wu, J. Compos. Mater. 5 (1971) 58–80.
[63] G.J. Dvorak, N. Laws, Eng. Fract. Mech. 25 (1986) 763–770.
[64] G.J. Dvorak, N. Laws, J. Compos. Mater. 21 (1987) 309–329.
[65] A. Wang, J. Compos. Technol. Res. 6 (1984) 45–62.
[66] D. Flaggs, J. Compos. Mater. 19 (1985) 29–50.
[67] P. Wanjara, R. Drew, S. Yue, Mater. Sci. Technol. 22 (2006) 61–71.
[68] R. Mahmudi, M. Sadeghi, J. Mater. Eng. Perform. 22 (2013) 433–438.
[69] M. Cheng, T. Wahafu, G. Jiang, W. Liu, Y. Qiao, X. Peng, T. Cheng, X. Zhang, G. He, X. Liu, Sci. Rep. 6 (2016) 1–14.
[70] C. Mu, Y. He, Y. Hu, M. Li, M. Chen, R. Wang, Y. Xiang, Z. Luo, K. Cai, Appl. Mater. Today 20 (2020) 100777.